Astron. Astrophys. 61, 199—215 (1977)

ASTRONOMY AND ASTROPHYSICS

# The Large and Small Magellanic Clouds in a Binary State, the Bending of the Galactic Disk and the Magellanic Stream

M. Fujimoto and Y. Sofue*
Department of Physics, Nagoya University, Nagoya 464, Japan

November 29, 1976

**Summary.** This paper consists of two parts: The first is a sequel to our earlier study of the tidal problem of the Galaxy and the Large and Small Magellanic Clouds (LMC and SMC). The second examines dynamically a primordial-gas model for the Magellanic Stream of hydrogen gas.

In the first part, we obtain several series of orbits for the LMC and SMC round the Galaxy, along which the two Clouds were in a binary state for the last 5 to $10 \times 10^9$ years. Approximately eight hundred test particles are distributed so as to simulate their continuous media within the Galaxy, LMC and SMC. The dynamical behavior of these particles is followed numerically and compared with the observed bending of the galactic disk and the Magellanic Stream. Two cases which assumes a galactic mass of $2.75\,10^{11}\,M_\odot$ and $1.40\,10^{11}M_\odot$ are examined. We conclude that if the bending of the disk is due to the tidal effect of the Magellanic Clouds, the total mass of our Galaxy (mass within 50 kpc of the galactic center) may be smaller than $2.7\,10^{11}\,M_\odot$, perhaps $\lesssim 2\,10^{11}\,M_\odot$.

From trials to reproduce the Magellanic Stream, high-velocity clouds (HVC) and other gas complexes ($l=270°$ to 330°, $b=-20°$ to 30°), we further conclude that the LMC and SMC orbits are on a plane perpendicular to the line joining the present position of the Sun and the galactic center ("overhead" attitude). Their peri- and apogalactocentric distances are 20 to 30 kpc and 50 to 60 kpc, respectively. Such trials fail, however, to reproduce the high negative radial velocity of the Magellanic Stream.

In the second part of our paper, we examine dynamically the primordial-gas model for the Stream proposed by Mathewson, Cleary and Murray (1974) and Mathewson (1976) to explain this velocity discrepancy and the positional coincidence of the Stream and most members of the Local Group.

**Key words:** the Galaxy — Magellanic Clouds — tidal interaction — bending — Magellanic Stream

## I. Introduction

Fujimoto and Sofue (1976; henceforth referred to as Paper I) obtained several series of orbits for the Large and Small Magellanic Clouds (LMC and SMC) passing the center of the Galaxy at 20, 30 and 40 kpc and along which the two Clouds were in a binary state for at least the past $5\,10^9$ years. The tidal interaction between the Galaxy, and the LMC and SMC in these binary orbits was estimated by following the motion of several hundred test particles distributed so as to simulate their continuous media within these galaxies.

The bending of the hydrogen gas layer in our Galaxy was reproduced if we chose a suitable LMC orbit whose perigalactic distance was 30 kpc. Furthermore, if the LMC orbit was in an overhead sense round the Galaxy, the test particles torn off tidally from the LMC and SMC formed a streak along a great circle on the sky, resembling the Magellanic Stream of Mathewson, Cleary and Murray (1974). We noted there, however, that the high negative velocity of hydrogen gas observed at/near the tip of the Stream ($l=90°$, $b=-35°$) could not be reproduced by this model. [See Kerr and Westerhout (1965), Henderson (1966), Kepner (1970), Davies (1972), Verschuur (1973) for observations of the bending structure; Elwert and Hablick (1965), Avner and King (1967), Hunter and Toomre (1969), Toomre (1972) for the theories of the bending; and Mathewson et al. (1974) and Mathewson (1976) for the Magellanic Stream.]

In Paper I, the orbital computations were made only for a single combination of the masses of the Galaxy, LMC and SMC, namely

$m_G=1.2\,10^{11}\,M_\odot$, $m_L=2\,10^{10}\,M_\odot$ and $m_S=2\,10^9\,M_\odot$.

It seemed likely, however, that such orbital computations would be sensitive not only to the masses of the Galaxy,

* Present address: Max-Planck-Institut für Radioastronomie, Auf dem Hügel 69, D-5300 Bonn 1, Federal Republic of Germany

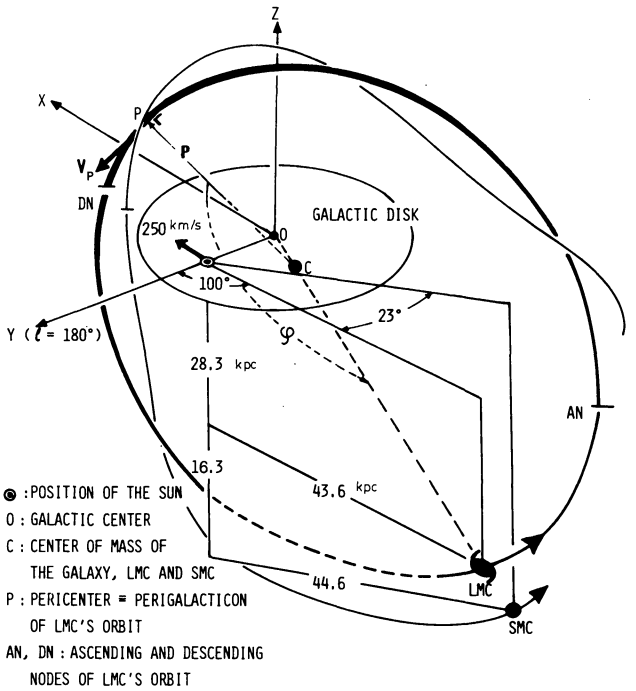


**Fig. 1.** Schematic bird's eye view of the geometrical relationship of the Galaxy, LMC and SMC (after Paper I). The center of mass is at $C$ and the $x$, $y$, $z$-axes are parallel to the $X$, $Y$, $Z$-axes. Positions of the Sun, LMC and SMC at present ($t=0$) are indicated

**Table 1**

| | |
|---|---|
| $t$: | The time reckoned from the present epoch ($t=0$ at present and $t>0$ for future). |
| $r(x, y, z)$: | The position vector in the center-of-mass system. |
| $r_G, r_L, r_S$: | The position vector of the Galaxy, LMC and SMC in the $(x, y, z)$ coordinate system. $r_G^0, r_L^0$ and $r_S^0$ are their present position vectors. |
| $D$: | The perigalactocentric distance of the LMC's orbit. |
| $v_L^0, v_S^0$: | The velocities of the LMC and SMC at $t=0$; their components are $v_L^0=(u_L, v_L, w_L)$ and $v_S^0=(u_S, v_S, w_S)$. |
| $\varphi$ | The angle between the LMC and its perigalacticon measured in the direction of revolution of the LMC. $\varphi_L^0$ is its value at $t=0$. |
| $(l, b)$: | The galactic longitude and latitude. |

**Table 2.** Observed kinematical quantities of the LMC and SMC

| $(l, b)$ | (280°, −33°) | (303°, −45°) |
|---|---|---|
| Distance from the Sun | 52 kpc | 63 kpc |
| Observed radial velocity corrected for the galactic rotation and the motion of the Sun in the LSR | 51 km s$^{-1}$ | 0 |
| Mass (assumed in the text) | $m_L=2\times10^{10}\,M_\odot$ and $10^{10}\,M_\odot$ | $2\times10^9\,M_\odot$ |

LMC and SMC and but also to our speed of the galactic rotation. This would be particularly apparent if a total mass for the Galaxy were chosen more than twice as large as the presently accepted value (Ostriker and Peebles, 1973). In the present paper we determine such effects in relation to our earlier results in Paper I. We also place limits on the total mass of the Galaxy by finding reasonable combinations of masses and other parameters of these three galaxies.

The basic postulate in Paper I, that the LMC and SMC are in a gravitationally bound state, is assumed here again. This postulate is based on the common diffuse gas around the LMC and SMC (Hindman, Kerr and McGee, 1963) and the polarization planes of bright stars and H II regions which are predominantly parallel to the line joining the Clouds (Mathewson and Ford, 1970; Schmidt, 1970).

Recently several other papers have appeared that claim the Magellanic Stream could be pulled out of these Clouds during a close encounter with the Galaxy, and that some dwarf galaxies and a few outlying galactic globular clusters are apparently associated with the Stream (Lynden-Bell, 1976). At the same time cautionary comments were made about the tidal theory and an alternative explanation was put forward that the diffuse gas clouds of the Stream are primordial, moving along the unbound hyperbolic orbit of the LMC about the galactic center (Mathewson and Schwarz, 1976). In the second part of this paper we discuss these two conflicting theories on the basis of our binary orbits of the Magellanic Clouds and of the test particles simulation.

The symbols and coordinates employed are the same as those used in Paper I, and are not repeated at length. Instead we reproduce a schematic bird's-eye view of the geometrical relationship of the Galaxy, LMC and SMC, with simple interpretations of some symbols in Fig. 1 and Table 1. Observed kinematical quantities of the LMC and SMC are presented in Table 2.

## II. Parameters of the Triple System of the Galaxy, LMC and SMC

Separate computations are made using the following three combinations of masses,

| Case I | Case II | Case III |
|---|---|---|
| $m_G=2.75\,10^{11}\,M_\odot$ | $2.75\,10^{11}\,M_\odot$ | $1.4\,10^{11}\,M_\odot$ |
| $m_L=2\,10^{10}$ | $10^{10}$ | $2\,10^{10}$ |
| $m_S=2\,10^9$ | $2\,10^9$ | $2\,10^9$ |

Case I: The mass of the Galaxy is taken as 2.3 times that taken in Paper I. This choice of mass is made not only to extend our earlier results but also to test the hypothesis that our Galaxy possess a massive halo. The mass of the LMC has been observationally estimated as $m_L=5\,10^9$ to $2\,10^{10}\,M_\odot$ (de Vaucouleurs, 1960; Hindman, Kerr and McGee, 1963; Hindman, 1967). In Case I we take $m_L=2\,10^{10}\,M_\odot$ as in Paper I; this value of $m_L$ is an upper value permitted by the present accuracy of observations.

Case II: We examine the case of an intermediate value $m_L=10^{10}\,M_\odot$, leaving other masses unaltered from

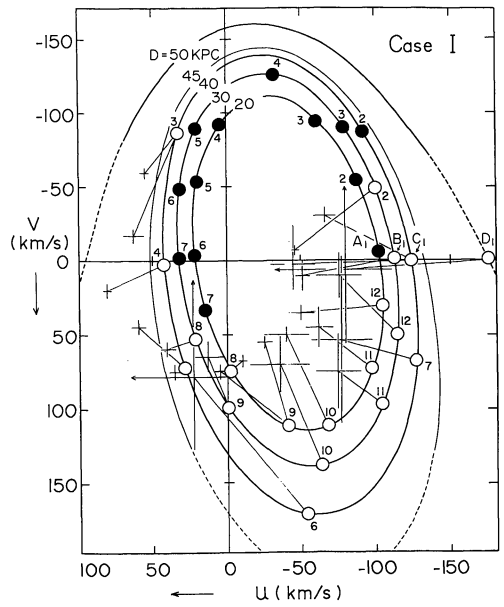


**Fig. 2a.** Possible velocities of the LMC $v_L^0$ and corresponding capture windows of the SMC for Case I. Our orbit-computations refer to $v_L^0$ at the small circles on the ellipses of $D=20$, 30, 40 and 50 kpc. The velocities of the LMC at the open circles ensure a binary state with the SMC for at least the past $5\,10^9$ years if the velocity of the SMC is suitably chosen in the capture window, which is represented by the cross joined with the assumed $v_L^0$ (see also Figure 3). The $z$-components of $v_L^0$ and $v_S^0$ are given by $w_L=-1.52\ u_L-0.268\ v_L-87.3$ and $w_S\approx-0.839\ u_s-0.545\ v_S$ km s$^{-1}$, respectively. The crosses joined with $C_6$ and $D_1$ show only the lower limits to the capture windows: Our orbit-surveys could not cover the whole capture windows. Note the directions of the $(u, v)$ coordinates, chosen for convenient reference to Figure 1

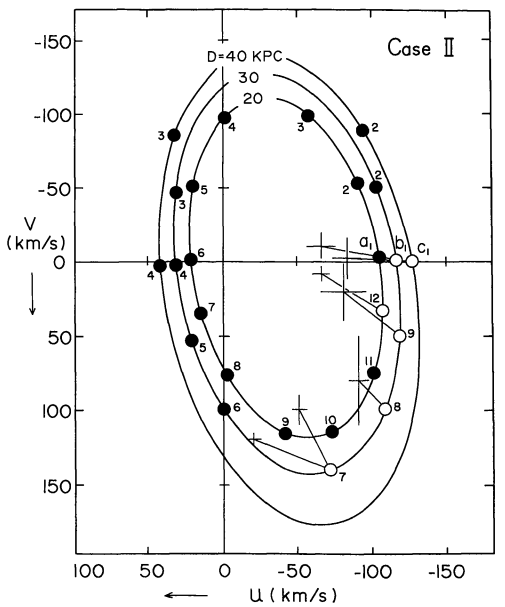


**Fig. 2b.** Same as Figure 2a, but Case II. $w_L=-1.52\ u_L-0.268\ v_L-84.1$ km s

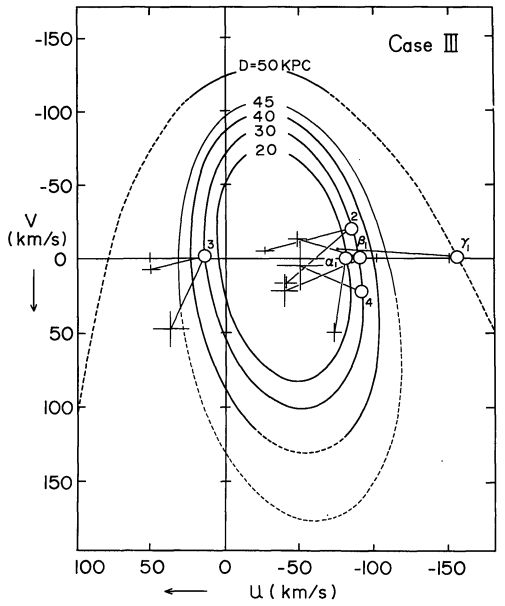


**Fig. 2c.** Same as Figure 2a, but Case III. $w_L=-1.52\ u_L-0.268\ v_L-81.9$ km s$^{-1}$

Case I, to see how the Magellanic dynamics depends on the mass of the LMC.

Case III: The mass of the Galaxy is nearly the same as in Paper I, but our rotation curve decreases more slowly outside the solar circle. This model was chosen to better reproduce the bending of the galactic disk and the Magellanic Stream. In all three cases, the rotation velocity of the Sun $V_\theta$ is taken as 250 km s$^{-1}$ and the distance of the Sun from the galactic center $R_0$ as 10 kpc.

Case IV: The fourth case of $V_\theta=225$ km s$^{-1}$ and $R_0=9$ kpc is only briefly discussed, associated with the bending structure of our Galaxy. The total mass of the Galaxy is almost the same as in Case III, $m_G=1.43\,10^{11} M_\odot$.

## III. Approximate Orbits of the LMC for the Last Several Billions of Years

As in Paper I, it proves convenient to know the approximate orbits of the LMC before entering into detailed computations of the three body problem of the Galaxy, LMC and SMC. Since $m_L \gg m_S$, we can estimate the orbit of the LMC in the near past without taking into account the SMC. If the LMC does not closely approach the galactic center, the gravitational potential due to the Galaxy can be approximately represented by a point-mass potential, which we assume in the present section to compute the approximate orbit of the LMC. Since the details of the orbit analysis were discussed in Paper I, we present immediately some orbital elements in Table 3 in the frame given in Fig. 1 for the assumed velocities of the LMC, $v_L^0$, at the present position (Figs. 2a to 2c), which, of course, satisfy the observed radial velocity. For all Cases I to IV, we assume a solar motion of 20 km s$^{-1}$ in the direction $l=56°$, $b=24°$. The listed velocities on the ellipses and the perigalactic distances of the LMC, $D=20$, 30, 40 and 50 kpc, agree exactly with the assumed

**Table 3.** Data on the orbits of the LMC* and the capture windows for the SMC

| I | II | | | III | | | IV | V | VI | VII | VIII |
|---|---|---|---|---|---|---|---|---|---|---|---|
| | $u_L^0$ (km s$^{-1}$) | | | $\boldsymbol{n}=(\boldsymbol{r}_L^0-\boldsymbol{r}_G^0)\times\boldsymbol{v}_L^0/\lvert(\boldsymbol{r}_L^0-\boldsymbol{r}_G^0)\times\boldsymbol{v}_L^0\rvert$ | | | $i$** | $\varphi_L^0$ | $\lvert r_L-r_G\rvert_{max}$ | Period ($10^9$ y) | Capture window |
| | ($u_L$, | $v_L$, | $w_L$) | ($n_x$, | $n_y$, | $n_z$) | | | | | |
| Case I | | | | | | | | | | | |
| $D=20$ kpc | | | | | | | | | | | |
| $A_1$ | −100.4 | − 5.4 | 67.1 | 0.002 | 0.997 | 0.083 | 94.8° | 150.0° | 58 | 2.7 | no |
| $A_2$ | − 85.4 | − 55.2 | 57.6 | −0.248 | 0.857 | 0.452 | 116.9 | 155.8 | 55 | 2.6 | no |
| $A_3$ | − 59.6 | − 93.2 | 28.7 | −0.451 | 0.513 | 0.731 | 137.0 | 160.5 | 54 | 2.5 | no |
| $A_4$ | 3.8 | − 92.0 | − 67.7 | −0.486 | −0.531 | 0.694 | 133.9 | 160.5 | 54 | 2.5 | no |
| $A_5$ | 19.7 | − 53.1 | −102.2 | −0.306 | −0.868 | 0.392 | 113.1 | 155.8 | 55 | 2.6 | no |
| $A_6$ | 21.8 | − 3.0 | −118.9 | −0.065 | −0.998 | 0.013 | 90.7 | 150.0 | 58 | 2.7 | no |
| $A_7$ | 15.1 | 34.1 | −118.7 | 0.117 | −0.958 | −0.261 | 74.9 | 145.8 | 60 | 2.9 | no |
| $A_8$ | − 2.1 | 76.3 | −103.9 | 0.327 | −0.758 | −0.564 | 55.7 | 141.2 | 64 | 3.0 | yes |
| $A_9$ | − 40.3 | 114.1 | − 56.0 | 0.527 | −0.217 | −0.822 | 34.7 | 137.2 | 68 | 3.3 | yes |
| $A_{10}$ | − 68.8 | 113.6 | − 12.7 | 0.542 | 0.238 | −0.806 | 36.3 | 137.2 | 68 | 3.3 | yes |
| $A_{11}$ | − 97.1 | 74.5 | 40.7 | 0.379 | 0.722 | −0.511 | 59.3 | 141.2 | 64 | 3.0 | yes |
| $A_{12}$ | −103.3 | 31.8 | 61.6 | 0.181 | 0.964 | −0.193 | 78.9 | 145.8 | 60 | 2.9 | yes |
| $D=30$ kpc | | | | | | | | | | | |
| $B_1$ | −111.1 | − 3.7 | 82.9 | 0.014 | 0.998 | 0.064 | 93.7 | 126.0 | 63 | 1.9 | yes |
| $B_2$ | − 98.4 | − 50.6 | 76.1 | −0.188 | 0.912 | 0.364 | 111.3 | 134.8 | 59 | 1.8 | yes |
| $B_3$ | − 77.1 | − 91.0 | 54.7 | −0.370 | 0.689 | 0.623 | 128.5 | 143.2 | 56 | 1.7 | no |
| $B_4$ | − 31.7 | −125.0 | − 5.3 | −0.542 | 0.102 | 0.834 | 146.5 | 150.9 | 54 | 1.7 | no |
| $B_5$ | 20.6 | − 89.0 | − 94.1 | −0.417 | −0.704 | 0.575 | 125.1 | 143.2 | 56 | 1.7 | no |
| $B_6$ | 31.4 | − 48.0 | −121.4 | −0.249 | −0.921 | 0.300 | 107.5 | 134.8 | 59 | 1.8 | no |
| $B_7$ | 32.0 | − 0.9 | −134.9 | −0.053 | −0.999 | −0.006 | 89.7 | 126.0 | 63 | 1.9 | no |
| $B_8$ | 21.1 | 52.9 | −132.8 | 0.172 | −0.924 | −0.341 | 70.1 | 117.0 | 70 | 2.2 | yes |
| $B_9$ | − 1.3 | 101.1 | −111.6 | 0.372 | −0.686 | −0.626 | 51.2 | 110.0 | 79 | 2.5 | yes |
| $B_{10}$ | − 64.0 | 139.8 | − 27.0 | 0.550 | 0.092 | −0.830 | 33.9 | 104.9 | 89 | 2.8 | yes |
| $B_{11}$ | −104.2 | 99.1 | 44.9 | 0.418 | 0.701 | −0.577 | 54.8 | 110.0 | 79 | 2.5 | yes |
| $B_{12}$ | −114.1 | 50.3 | 73.1 | 0.234 | 0.932 | −0.276 | 74.0 | 117.0 | 70 | 2.2 | yes |
| $D=40$ kpc | | | | | | | | | | | |
| $C_1$ | −122.1 | − 0.41 | 98.6 | 0.030 | 0.999 | 0.041 | 92.3 | 83.1 | 81 | 1.9 | yes |
| $C_2$ | − 89.7 | − 88.4 | 73.0 | −0.316 | 0.744 | 0.548 | 123.3 | 105.6 | 62 | 1.4 | no |
| $C_3$ | 32.5 | − 86.0 | −112.9 | −0.369 | −0.787 | 0.494 | 119.6 | 105.6 | 62 | 1.4 | no |
| $C_4$ | 42.1 | 2.8 | −151.2 | −0.037 | −0.999 | −0.029 | 88.3 | 83.1 | 81 | 1.9 | yes |
| $C_5$ | 28.2 | 74.0 | −149.1 | 0.213 | −0.891 | −0.401 | 66.4 | 71.8 | 113 | 2.6 | yes |
| $C_6$ | − 53.5 | 173.5 | − 51.8 | 0.544 | −0.082 | −0.835 | 33.4 | 61.5 | 263 | 7.4 | yes |
| $C_7$ | −126.5 | 70.9 | 86.3 | 0.273 | 0.900 | −0.339 | 70.2 | 71.8 | 113 | 2.6 | yes |
| $D=50$ kpc | | | | | | | | | | | |
| $D_1$ | −177.0 | − 0.16 | 181.9 | 0.034 | 0.999 | 0.034 | 91.9 | 16.5 | ∞ | ∞ | yes |
| Case II | | | | | | | | | | | |
| D=20 kpc | | | | | | | | | | | |
| $a_1$ | −103.2 | − 4.2 | 67.9 | 0.008 | 0.997 | 0.074 | 94.2 | 149.3 | 58 | 2.7 | no |
| $a_2$ | − 88.8 | − 53.6 | 59.3 | −0.235 | 0.870 | 0.433 | 115.7 | 155.0 | 56 | 2.6 | no |
| $a_3$ | − 56.3 | − 99.2 | 22.5 | −0.474 | 0.443 | 0.761 | 139.6 | 160.6 | 54 | 2.5 | no |
| $a_4$ | − 0.6 | − 98.1 | − 62.6 | −0.505 | −0.426 | 0.729 | 136.8 | 160.6 | 54 | 2.5 | no |
| $a_5$ | 19.8 | − 51.4 | −106.0 | −0.294 | −0.880 | 0.372 | 111.8 | 155.0 | 56 | 2.6 | no |
| $a_6$ | 21.4 | − 1.8 | −121.7 | −0.059 | −0.998 | 0.004 | 90.2 | 149.3 | 58 | 2.7 | no |
| $a_7$ | 14.6 | 35.4 | −121.3 | 0.120 | −0.957 | −0.265 | 74.6 | 145.2 | 61 | 2.9 | no |
| $a_8$ | − 2.8 | 77.8 | −106.2 | 0.327 | −0.758 | −0.564 | 55.7 | 140.7 | 64 | 3.1 | no |
| $a_9$ | − 40.7 | 115.9 | − 58.9 | 0.525 | −0.232 | −0.819 | 35.0 | 136.8 | 68 | 3.3 | no |
| $a_{10}$ | − 71.6 | 115.3 | − 11.9 | 0.541 | 0.253 | −0.802 | 36.7 | 136.8 | 68 | 3.3 | no |
| $a_{11}$ | − 99.5 | 75.9 | 41.0 | 0.379 | 0.772 | −0.510 | 59.3 | 140.7 | 64 | 3.1 | no |
| $a_{12}$ | −105.9 | 33.0 | 62.1 | 0.184 | 0.963 | −0.198 | 78.6 | 145.2 | 61 | 2.9 | yes |
| $D=30$ kpc | | | | | | | | | | | |
| $b_1$ | −114.2 | − 1.0 | 83.9 | 0.026 | 0.999 | 0.047 | 92.7 | 124.7 | 64 | 2.0 | yes |
| $b_2$ | −101.3 | − 50.2 | 77.4 | −0.182 | 0.917 | 0.356 | 110.9 | 133.7 | 59 | 1.8 | no |
| $b_3$ | 31.4 | − 47.6 | −124.6 | −0.244 | −0.925 | 0.292 | 107.0 | 133.7 | 59 | 1.8 | no |
| $b_4$ | 31.6 | 1.9 | −138.1 | −0.041 | −0.999 | −0.023 | 88.7 | 124.7 | 64 | 2.0 | no |
| $b_5$ | 21.0 | 53.6 | −135.8 | 0.170 | −0.925 | −0.339 | 70.2 | 116.4 | 71 | 2.2 | no |

**Table 3** (continued)

| I | II | | | III | | | IV | V | VI | VII | VIII |
|---|---|---|---|---|---|---|---|---|---|---|---|
| | $u_L^0$ (km s$^{-1}$) | | | $n=(r_L^0-r_G^0)\times v_L^0/\lvert(r_L^0-r_G^0)\times v_L^0\rvert$ | | | $i$** | $\varphi_L^0$ | $\lvert r_L-r_G\rvert_{max}$ | Period ($10^9$ y) | Capture window |
| | ($u_L$, | $v_L$, | $w_L$) | ($n_x$, | $n_y$, | $n_z$) | | | | | |
| $b_6$ | − 1.5 | −102.3 | −114.7 | 0.369 | −0.691 | −0.621 | 51.6 | 109.5 | 80 | 2.5 | no |
| $b_7$ | − 70.4 | 141.4 | − 20.8 | 0.548 | 0.152 | −0.822 | 34.7 | 104.4 | 90 | 2.8 | yes |
| $b_8$ | −107.1 | 100.2 | 45.9 | 0.416 | 0.707 | −0.573 | 55.0 | 109.5 | 80 | 2.5 | yes |
| $b_9$ | −116.9 | 50.9 | 74.1 | 0.233 | 0.933 | −0.274 | 74.1 | 116.4 | 71 | 2.2 | yes |
| $D=40$ kpc | | | | | | | | | | | |
| $c_1$ | −125.1 | − 0.6 | 100.3 | 0.029 | 0.999 | 0.042 | 92.4 | 82.3 | 82 | 1.9 | yes |
| $c_2$ | − 92.8 | − 89.0 | 74.8 | −0.312 | 0.781 | 0.542 | 122.8 | 103.9 | 62 | 1.5 | no |
| $c_3$ | 32.9 | − 86.5 | −116.4 | −0.364 | −0.794 | 0.487 | 119.1 | 103.9 | 62 | 1.5 | no |
| $c_4$ | 42.4 | 2.7 | −154.6 | −0.038 | −0.999 | −0.028 | 88.4 | 82.3 | 82 | 1.9 | no |
| Case III | | | | | | | | | | | |
| $D=20$ kpc | | | | | | | | | | | |
| $\alpha_1$ | − 80.4 | − 0.5 | 40.7 | 0.021 | 0.998 | 0.054 | 93.1 | 139.7 | 65 | 3.1 | yes |
| $D=30$ kpc | | | | | | | | | | | |
| $\beta_1$ | − 88.4 | − 0.8 | 52.9 | 0.022 | 0.998 | 0.052 | 93.0 | 111.6 | 77 | 2.4 | yes |
| $\beta_2$ | − 83.6 | − 21.7 | 51.1 | −0.104 | 0.965 | 0.241 | 103.9 | 116.1 | 71 | 2.2 | yes |
| $\beta_3$ | 13.5 | 1.3 | −102.1 | −0.044 | −0.999 | −0.018 | 89.0 | 111.6 | 77 | 2.4 | yes |
| $\beta_4$ | − 90.7 | 22.0 | 50.4 | 0.153 | 0.977 | −0.150 | 81.4 | 107.2 | 84 | 2.6 | yes |
| $D=50$ kpc | | | | | | | | | | | |
| $\gamma_1$ | −155.4 | − 1.18 | 154.7 | 0.031 | 0.999 | 0.039 | 92.2 | 15.0 | ∞ | ∞ | yes |
| Case IV | | | | | | | | | | | |
| $D=20$ kpc | | | | | | | | | | | |
| | − 81.0 | − 0.03 | 41.3 | 0.014 | 1.000 | 0.028 | 91.6 | 140.2 | 64 | 3.1 | yes |
| $D=30$ kpc | | | | | | | | | | | |
| | − 89.0 | 0.2 | 53.6 | 0.016 | 1.000 | 0.025 | 91.4 | 112.2 | 76 | 2.3 | yes |

* The orbital elements of the LMC in the point-mass potential in Section III, except for the eighth column. In the three-body problem in the potentials (1) and (2) in Section IV, however, the maximum distance between the Galaxy and LMC often exceeds the values in the sixth column by ten to twenty percent.

** Inclination of $\boldsymbol{n}$ relative to the rotation axis of the Galaxy: $0 \leqq i < 90°$; direct revolution; $i=90°$, overhead; and $90° \leqq i \leqq 180°$, retrograde

point-mass potential of the Galaxy. Some representative values of $\boldsymbol{v}_L^0$ are shown by circles on the ellipses and the orbital elements specified by these points are given in Table 3. When the circles are on the dashed lines in Figs. 2, the LMC's orbits are hyperbolic, and the LMC is unbound to the Galaxy. Furthermore, when the $y$-component of $\boldsymbol{v}_L^0$ is zero or much smaller than the other two components, the LMC's orbits are in an overhead sense round the Galaxy and the orbital plane is normal to the line joining the Sun and the galactic center.

As is discussed in Section IV, such overhead orbits best reproduce the Magellanic Stream, the high-velocity clouds (HVC) and the bending of our galactic disk (Paper I). Amongst them, an overhead hyperbolic orbit with $D=50$ kpc was proposed by Mathewson (1976) in order to account for both the geometry and the radial velocities of the Magellanic Stream. When $m_G=1.2\,10^{11}\,M_\odot$ (Paper I) to $2.75\,10^{11}\,M_\odot$, this orbit is obtained. If Mathewson's model orbit is correct, the LMC passed its perigalacticon in the near past and is moving away now from us. In this case, however, the bending of our galactic disk can never be reproduced by the tidal force from the Magellanic Clouds (Section V). Hence, we would need to search for another mechanism to warp the galactic disk.

From their overall study of the Local Group of galaxies, Einasto, Haud, Joever and Kaasik (1976) proposed an elliptical orbit of the LMC whose peri- and apogalactocentric distances are respectively 14 and 100 kpc, but their orbit is not permitted from Fig. 2 in Paper I and Figs. 2a to 2c and Table 3. Furthermore, we have concluded in Paper I that an approach of the LMC as close as 14 kpc to the galactic center would cause too large a noncircular motion ($>50$ km s$^{-1}$) in the solar neighborhood.

## IV. Three Body Problem of the Galaxy, LMC and SMC

The point-mass potential we have previously used is inadequate for simulating the evolution of the actual

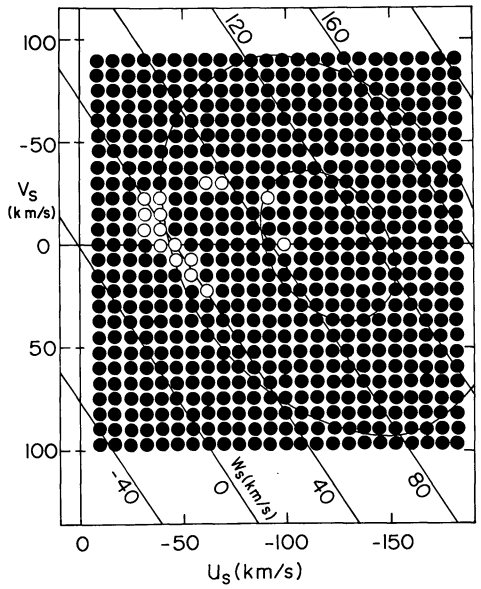


**Fig. 3a.** Orbit computations of the SMC made for about 600 choices of $v_S^0$ from point $C_1$ in Figure 2a. The outer and inner ellipses refer to $|v_S^0 - v_L^0| = 100$ and 40 km s$^{-1}$, respectively. The capture window defined by the open circles is given approximately also by the cross in Figure 2a. Note again the $(u_S, v_S)$ coordinates

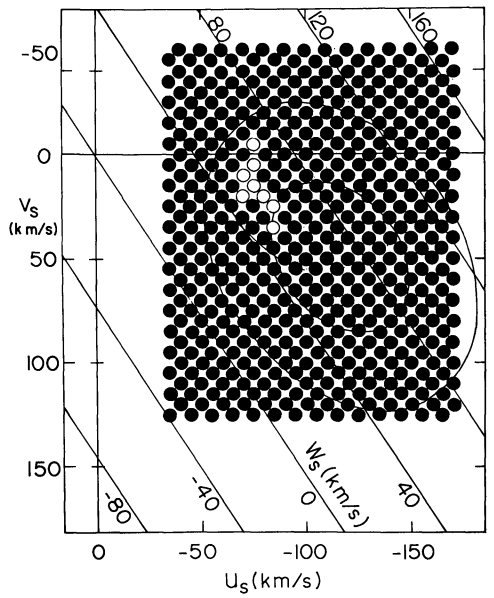


**Fig. 3b.** Same as Figure 3a, but the LMC velocity $v_L^0$ corresponds to $B_{12}$ in Figure 2a. The inner and outer ellipses refer to $|v_S^0 - v_L^0| = 40$ and 80 km s$^{-1}$

triple system of the Galaxy, LMC and SMC. We therefore assume here a generalized Kuzmin-Toomre type potential (Miyamoto and Nagai, 1975; Nagai and Miyamoto, 1976)

$$\Phi_G = \sum_{i=1}^{2} \frac{Gm_i}{[R^2+(a_i+\zeta_i)^2]^{1/2}} \cdot \left\{1 + \frac{a_i(a_i+\zeta_i)}{R^2+(a_i+\zeta_i)^2} - \frac{1}{3}\frac{a_i^2[R^2-2(a_i+\zeta_i)^2]}{[R^2+(a_i+\zeta_i)^2]^2}\right\}, \quad (1)$$

with

$$\zeta_i = (Z^2+b_i^2)^2 \quad \text{and} \quad R^2 = X^2+Y^2,$$

where $G$ is the gravitational constant. The constants $m_1$, $m_2$ ($m_G = m_1+m_2$), $a_1$, $a_2$, $b_1$ and $b_2$ are so chosen that $\Phi_G$ reproduces the rotation velocity on the galactic plane and the velocity dispersion of stars near the sun.

For the potentials of the LMC and SMC, we follow Plummer's (1911) law as in Paper I,

$$\Phi_{L,S} = Gm_{L,S}/[(r-r_{L,S})^2 + K^2{}_{L,S}]^{1/2}, \quad (2)$$

where $K_L = 3$ kpc for the LMC and $K_S = 2$ kpc for the SMC. Equations of motion for the whole system, in the reference coordinate system with its origin at the center-of-mass of these three galaxies, are then

$$\ddot{r}_i = \frac{\partial}{\partial r_i}\sum_{j\neq i}\Phi_j(|r_i - r_j|), \quad (3)$$

where the suffices $i$ and $j$ represent the three galaxies, and $\Phi_j$ the gravitational potential due to the $j$-th galaxy.

The past orbits of the LMC and SMC can be determined by integrating equation (3) backward from the present epoch ($t=0$) with the initial conditions of the LMC and SMC satisfying their present observed positions and radial velocities. For the LMC we can take a point in Figure 2a to 2c as a reasonable approximation. (The $z$-component of $v_L^0$ is evaluated as $w_L = -1.52\,u_L - 0.27\,v_L - 93.6\,m_G/(m_L+m_G)$ in km s$^{-1}$ by equation (7) in Paper I. Lines of constant value of $w_L$ given in Figure 2 in Paper I are deleted here in order to avoid complicated figures). For the SMC we can take a point on the $(u_S, v_S, w_S)$-plane in Figures 3a and 3b, for example, as an acceptable initial value.

The orbit computations are extended backward through time until $t = -10^{10}$ years for various initial values $v_L^0$ indicated by the circles on the ellipses in Figures 2a to 2c; corresponding numerous initial values $v_S^0$ are taken, such as are indicated by the circles in Figures 3a and 3b. In the majority of cases indicated by filled circles, the calculations reveal that the LMC and SMC could not be bound to each other in the very remote past. However, we found that certain specific choices of $v_S^0$ for these assumed $v_L^0$ do permit a binary state of the two Clouds over at least the past $5\,10^9$ years. These present velocities $v_L^0$ have been indicated by the open circles in Figures 2.

*Case I*

We begin with the case of $m_G = 2.75\,10^{11}\,M_\odot$, $m_L = 2\,10^{10}\,M_\odot$ and $m_S = 2\,10^9\,M_\odot$. The parameters of the Galaxy potential (1) are: $a_1 = 0$, $a_2 = 7.26$ kpc, $b_1 = 0.495$ kpc, $b_2 = 0.520$ kpc, $m_1 = 2\,10^{10}\,M_\odot$, and $m_2 = 2.55\,10^{11}\,M_\odot$ or $m_G = m_1+m_2 = 2.75\,10^{11}\,M_\odot$ (Miyamoto and Nagai, 1975). The orbit computations were made for the thirty two initial velocities $v_L^0$ at the circles $A_1, A_2, \ldots, D_1$ on the ellipses of $D = 20$, 30, 40 and 50 kpc, for each of which about 600 velocities $v_S^0$ were

assumed such as illustrated in Figures 3a and 3b. The "capture windows" thus obtained for the SMC velocities are given in the form of crosses joined to the corresponding $v_L^0$ in Figures 2. Note that every velocity in Figures 2 and 3 is referred to the center-of-mass system.

As shown in Figure 4a, when we choose $v_S^0$ corresponding to about the middle of the capture window in Figure 3a, the LMC and SMC accompany each other throughout the past $10^{10}$ years. When we choose $v_S^0$ outside the capture window, binary structure is disrupted within the past $5\,10^9$ years (Figure 4b), mostly within the past 2 to $3\,10^9$ years. Since $m_L \ll m_G$, the LMC always maintains an approximately periodic motion. The inclination of the orbital plane and the position of the perigalacticon $\varphi_L^0$ of the LMC are given in the eighth and ninth column in Table 3.

We have often encountered complicated orbits whose binary structure is difficult to judge. Therefore we decided that the system is not binary if the distance between the LMC and SMC exceeds even slightly the mean distance between the Galaxy and the LMC, $|r_L - r_S| \gtrsim \{\max(|r_G - r_L|) + \min(|r_G - r_L|)\}/2$. For example, the orbits in Figure 4b are not regarded as binary for more than the past $5\,10^9$ years.

When $D = 40$ and 50 kpc, the tidal force from the Galaxy is much reduced on the LMC-SMC system and the capture window becomes wider. We computed only the orbits which circle our Galaxy in an approximately overhead sense. Particularly when $D = 50$ kpc, the orbits are hyperbolic, unbound to the Galaxy. These orbits will be used in the latter part of the present paper, concerning a new model for the Magellanic Stream of Mathewson (1976).

The LMC and SMC could have been in a binary state for the past $5\,10^9$ years and rarely the entire $10^{10}$ years, if the LMC's velocity is at the open circle on the $D = 20$ to 50 kpc ellipses in Figure 2a and if the SMC's velocity is chosen to lie in the capture window. It hardly needs to be added here that, since the spacings between the neighboring points in Figure 3 are taken as 7.5 km s$^{-1}$ or 5 km s$^{-1}$ if necessary in $u_S$, $v_S$ and $w_S$, the capture windows are not mathematically strict but have uncertainties of this magnitude. We cannot guarantee that no open circles exist between those in the $(u_S, v_S, w_S)$-space in Figure 3 but their existence seems quite unlikely. The distribution pattern of the capture window in the $(u_S, v_S, w_S)$-space may perhaps be understood in the same way as in Paper I (p. 245).

Since we have been concerned with a Galaxy of $m_G = 2.75\,10^{11}\,M_\odot$, 2.3 times that taken in Paper I ($m_G = 1.2\,10^{11}\,M_\odot$), the tidal force on the LMC-SMC system is correspondingly larger and consequently the capture windows are much narrowed and occasionally even disappear. In fact, the arcs of the ellipses covering the open circles become much shorter than those in Paper I. The probability that the Clouds have been in a binary state is much larger for $m_G = 1.2\,10^{11}\,M_\odot$ than for

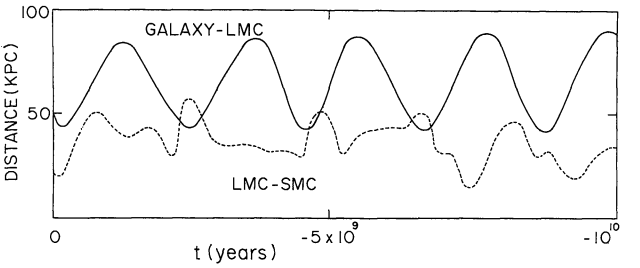


**Fig. 4a.** Distances between the galactic center and LMC and between the LMC and SMC as a function of time. Case I is considered. $v_L^0$ is at $C_1$ in Figure 2a and $v_S^0 = (42.5, 15.0, 44.1)$ km s$^{-1}$ in Figure 3a

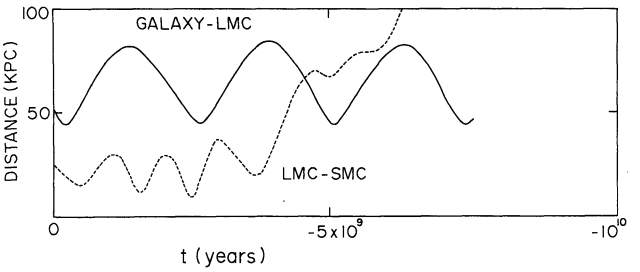


**Fig. 4b.** Same as Figure 4a, but $v_S^0 = (95.0, 15.0, 88.1)$ km s$^{-1}$ outside the capture window. When the SMC remains bound to the Galaxy, it is sometimes difficult to estimate a binary state. Here we consider that the LMC-SMC system is not a binary if $|r_L - r_S| \geqq \{\max(|r_L - r_G|) + \min(|r_L - r_G|)\}/2$ is realized. Accordingly, the LMC-SMC system in this figure is regarded as disrupted before $5\,10^9$ years ago

$m_G = 2.75\,10^{11}\,M_\odot$, but at present we cannot say which mass is the more realistic.

*Case II*

The mass of the LMC is reduced to $10^{10}\,M_\odot$. Other kinematical parameters and orbit-calculations backward through time remain the same as in Case I. The adopted initial velocities $v_L^0$ and the resultant capture windows are given together in Figure 2b. (The $z$-components of $v_L^0$ and $v_S^0$, $w_L$ and $w_S$, are evaluated as in Case I.)

Since the binding energy of the two Clouds is reduced compared with that for Case I, the corresponding capture windows are much narrowed and many of them disappear occasionally. Indeed, a comparison of Figures 2a and 2b shows such tendency particularly for the circles on the $D = 20$ and 30 kpc ellipses. However, the positions of the capture windows of the SMC relative to the corresponding $v_L^0$ remain qualitatively the same.

We can confirm that the capture windows for the SMC orbits are greatly dependent on the mass of the LMC. For example, if $m_G \cong 2.7\,10^{11}\,M_\odot$ and $m_L \lesssim 10^{10}\,M_\odot$, the probability that the LMC and SMC were in a binary state and passed the center of our Galaxy at $D = 20$ kpc becomes extremely small; if $m_G \gtrsim 3\,10^{11}\,M_\odot$ (the mass within 50 kpc of the Galaxy) and $m_L \lesssim 5\,10^9\,M_\odot$, the hypotheses that the Magellanic Clouds revolve round the Galaxy with $D = 20$ kpc can certainly be ruled out.

It is still difficult however to provide an upper limit of the mass of the Galaxy from these results alone. For such an estimate we must rely, as in Paper I, upon other dynamical phenomena that would be associated with the LMC and SMC. The following sections V and VI are devoted to this problem.

*Case III*

The parameters specifying the Galaxy potential (1) are: $a_1=0$, $a_2=11.0$ kpc, $b_1=0.50$ kpc, $b_2=0.34$ kpc, $m_1=2.0\,10^{10}\,M_\odot$ and $m_2=1.2\,10^{11}\,M_\odot$ or $m_G=m_1+m_2=1.4\,10^{11}\,M_\odot$ (Nagai and Miyamoto, 1976). The choice of the Galaxy mass ($1.4\,10^{11}\,M_\odot$) is made so as to reproduce simultaneously both the bending of the hydrogen gas layer in the Galaxy and the Magellanic Stream, with the hope reconciling our computed bending with the observations on the latituderadial velocity or $(v_r-b)$ diagrams (Henderson, 1966) ($v_r$ and $b$ denote the radial velocity and galactic latitude, respectively). In Paper I the computed bending was comparable to observations in magnitude and sense, but no satisfactory coincidence was obtained on the $(v_r-b)$ diagrams (see Figure 9 in Paper I). We thought it due to our adopted Innanen's (1966) model Galaxy (model 252-10 in his terms) whose rotation velocity decreases steeply outside the solar circle.

The search for the capture windows here was done for the velocities only at $\alpha_1$ on the $D=20$kpc ellipse, $\beta_1$ to $\beta_4$ on the $D=30$ kpc ellipse and $\gamma_1$ on the $D=50$ kpc ellipse (Figure 2c). This is because we are interested in reproducing the bending of our galactic disk and the Magellanic Stream due to the LMC and SMC circling the Galaxy in an overhead sense. The capture windows are approximately the same as those in Paper I.

*Case IV*

$R_0=9$ kpc and $V_\theta=225\,\mathrm{km\,s^{-1}}$ are often quoted as possible galactic constants. We assumed $a_1=0$, $a_2=3.7$ kpc, $b_1=0$ and $b_2=0.5$ kpc in equation (1), or $m_G=1.43\,10^{11}\,M_\odot$, only two percent larger than that of Case III. In order to examine the bending structure in this Galaxy model, we tried to find some binary orbits of the LMC and SMC circling our Galaxy in an overhead sense with $D=20$ and 30 kpc. The capture windows in the $v_S^0$-space are almost the same as in Case III.

## V. Tidal Distortion of the Galaxy by the Magellanic Clouds

In order to estimate the distortion of the galactic disk due to the close passage of the Magellanic Clouds, we simulate the galactic disk by five hundred test particles rotating in the potential (1), and we follow their noncircular and nonplannar motion caused mostly by the LMC.

Our procedure is the same as in Paper I, closely resembling various test-particle studies by Pfleider and Siedentopf (1961), Pfleider (1963), Yabushita (1971), Clutton-Brock (1972), Toomre and Toomre (1972), Wright (1972), and Eneev, Kozlov and Sunyaev (1973). The exploratory orbits of the LMC and SMC used in the following sections are taken from among those that guarantee a binary structure for at least the past $5\,10^9$ years.

The equation of motion of a test particle is then

$$\frac{d^2\boldsymbol{r}}{dt^2}=\frac{\partial}{\partial r}\Phi_G(|\boldsymbol{r}-\boldsymbol{r}_G|)-\frac{Gm_L(\boldsymbol{r}-\boldsymbol{r}_L)}{[(|\boldsymbol{r}-\boldsymbol{r}_L|)^2+K_L^2]^{3/2}}-\frac{Gm_S(\boldsymbol{r}-\boldsymbol{r}_S)}{[(|\boldsymbol{r}-\boldsymbol{r}_S|)^2+K_S^2]^{3/2}}, \tag{4}$$

where $\Phi_G(|\boldsymbol{r}-\boldsymbol{r}_G|)$ is the gravitational potential (1). By definition the gravitational interaction between the test particles is negligible. The position of the LMC and SMC, $\boldsymbol{r}_L$ and $\boldsymbol{r}_S$ in equation (4), are regarded as given functions of time. These test particles were initially located on discrete rings. Here we choose to employ eleven rings, and to place them at equally-spaced radii from $R=6$ kpc to 15 kpc on the galactic plane. An initial circular motion was given to each particle so that the centrifugal force exactly balances the gravitational force of the Galaxy.

Again we report separately the numerical simulations carried out for the three Cases I, II and III.

*Case I*

The tidal distortions of the sheet of test particles were followed mostly for the LMC orbits in an overhead sense round the Galaxy with $D=20$ and 30 kpc. The integration of equation (4) started, in effect, at the instant when the LMC passed the apogalacticon and was performed toward the present ($t=0$).

Since the assumed mass of our Galaxy, $m_G=2.75\,10^{11}\,M_\odot$, is more than twice that in Paper I, the tidal damage is correspondingly slight. Nevertheless, spiral structures due to the horizontal noncircular motion are produced as in other numerical works by many authors cited above. Bending of the sheet of test particles also takes place although its amplitude is quite small: by $t=0$, they amount to, at most, $|\Delta Z|\cong 150$ pc at $R=18$ kpc, $|\Delta Z|=100$ pc at $R=14$ kpc and $|\Delta Z|\leqq 50$ pc at the solar circle. The sense of the bendings, $\Delta Z<0$ for the disk facing the Magellanic Clouds and $\Delta Z>0$ for the opposite, is compatible with observations.

The amplitudes of the bending are, however, obviously incompatible with observations. In order to remedy this, we tried the same computations for the LMC orbit in a direct sense with respect to the rotation of the Galaxy, characterized by the point $A_{11}$ on the $D=20$ kpc ellipse in Figure 2a. However, no satisfactory result was obtained. For the LMC orbit of $D\geqq 30$ kpc, of course, we could not reproduce bending structures with amplitudes comparable to observations.

In the discussions of the vertical distortions, we must remember that the gravitational potential of our model Galaxy was adopted beforehand and was assumed to remain unchanged during the bending of the disk. The restoring force of the bent disk upon the particles is, therefore, larger than that of a self-gravitating disk. It tends to result in an underestimate of amplitudes in the present numerical studies. On the other hand, we have defined vertical amplitude as the displacement of the particles from an invariant plane. Yet, as Hunter and Toomre (1969) stressed, the observed bending amplitude refers to a galactic disk in which the Sun is located and which itself would already have been tilted appreciably by the tidal force from the LMC. Even if we take these effects into account, however, the computed bending $|\Delta z|$ is still too small to be compared to the observed flexure.

*Case II*

From the results in Case I, we can confidently conclude without further numerical computations that the bending of our galactic disk in the present Case cannot be produced by the tidal force from the LMC whose mass is less than $10^{10} M_\odot$ and whose nearest approach to the Galaxy is more than 20 kpc.

The results in Cases I and II lead to the conclusion that if the total mass of the Galaxy (within 50 kpc from its center) is more than $2.75\,10^{11} m_\odot$ (2.3 times that in Paper I) and if the LMC and SMC have been in a binary state, the bending of our galactic plane must be caused by another, non-tidal force. Alternatively, if the bending is due to the tidal force, the large-mass model of the Galaxy (Ostriker and Peebles, 1973) must be rejected. We stress that the current controversy concerning the mass of our Galaxy is but part of a much larger problem involving the mass of the LMC, the mechanism of the bending of the galactic disk, and also the dynamical model of the Magellanic Clouds—whether they are a steady binary circling round the Galaxy or are accidental passers-by on hyperbolic orbits.

*Case III*

The tidal distortions of the Galaxy are determined exclusively for the LMC orbits revolving in an overhead attitude with $D=20$ and 30 kpc. Since the computations are the same as in Case I, we give immediately the results of the bending on the $(v_r, b)$ diagrams, in comparison with observations by Henderson (1966).

We anticipated better reproductions of the bending structure by introducing a model Galaxy whose rotation velocity decreases more slowly beyond the solar circle than that of Innanen's model Galaxy in Paper I. As shown in Figures 5a and 5b, some qualitative agreements with observations are found, particularly for the outer parts of the disk, but the displacement of test particles in the intermediate ranges of the radial velocity, $-80 \lesssim v_r \lesssim -30\ \mathrm{km\,s^{-1}}$ in $l=30°$ and $-160 \lesssim v_r \lesssim -60\ \mathrm{km\,s^{-1}}$ in $l=90°$ (Figs. 5a and 5b) is still not entirely satisfactory. We tried the same computations for the model Galaxy of Case IV; $R_0=9$ kpc, $V_\theta=225\ \mathrm{km\,s^{-1}}$ and $m_G=1.43\,10^{11} M_\odot$ (Figures 6a and 6b). A slight improvement is found, but the computed bending and their discrepancy from observations are essentially the same as in Case III. (See also Toomre's (1972) discussions on $R_0$ and $V_0$ in this context.) The test particles in Figures 5 and 6 are distributed in several groups along the abscissae represent spiral condensations viewed in these directions.

If a comparison is allowed between our computed *outer* bendings and the observations of H I gas, a reasonable combination of kinematical parameters, namely $20 \lesssim D \lesssim 30$ kpc, $m_G < 2\,10^{11} M_\odot$ (within about 50 kpc from the galactic center) and $m_L > 10^{10} M_\odot$ are obtained. The value of $m_L$ will perhaps be near $2\,10^{10} M_\odot$. It is still difficult however to make a definite choice between our two galactic models, Case III and IV.

The bending in the intermediate ranges of the radial velocity on the $(v_r, b)$-plane cannot be improved simply by adopting the model Galaxy of Case III. Neglected factors such as the self-gravity of the disk and the definition of the reference plane for the bending might, as we mentioned in Case I, contribute to such unsatisfactory results. Our present study, however, cannot throw any further light on these problems.

## VI. Tidal Effect of the Galaxy on the Magellanic Clouds

We turn our attention to the dynamical behavior of matter in and around the LMC and SMC under the tidal influence of the Galaxy. Observational as well as theoretical arguments have already been made about the tidal disruptions of the outer parts of the Clouds and the debris that would be observed emerging from them (Mirable and Turner, 1973; Clutton-Brock, 1972; Toomre, 1973, and Mathewson, Cleary and Murray, 1974). The discovery of the "Magellanic Stream" of hydrogen gas (Warnnier and Wrixon, 1972; Mathewson et al., 1974) seemed to provide support for the above theoretical predictions. In Paper I we made use of such results, enabling more probable orbits of the LMC and SMC to be selected from the large number of binary-orbits determined in the preceding sections. [For earlier references to the discovery of the Stream, see Dieter (1965), Hulsbosh and Raimond (1966), and van Kuilenburg (1972)].

More recently, Mathewson (1976) proposed that the Magellanic Stream is a band of primordial gaseous debris left from the formation of the Clouds and moving along a hyperbolic orbit unbound to the Galaxy. The HVCs which are observed on a great circle defined by the Magellanic Stream should be then regarded as different objects. This new model promises to explain the observed radial velocity of the Stream. Indeed, the high negative radial velocity near the tip of the Stream ($l=90°$,

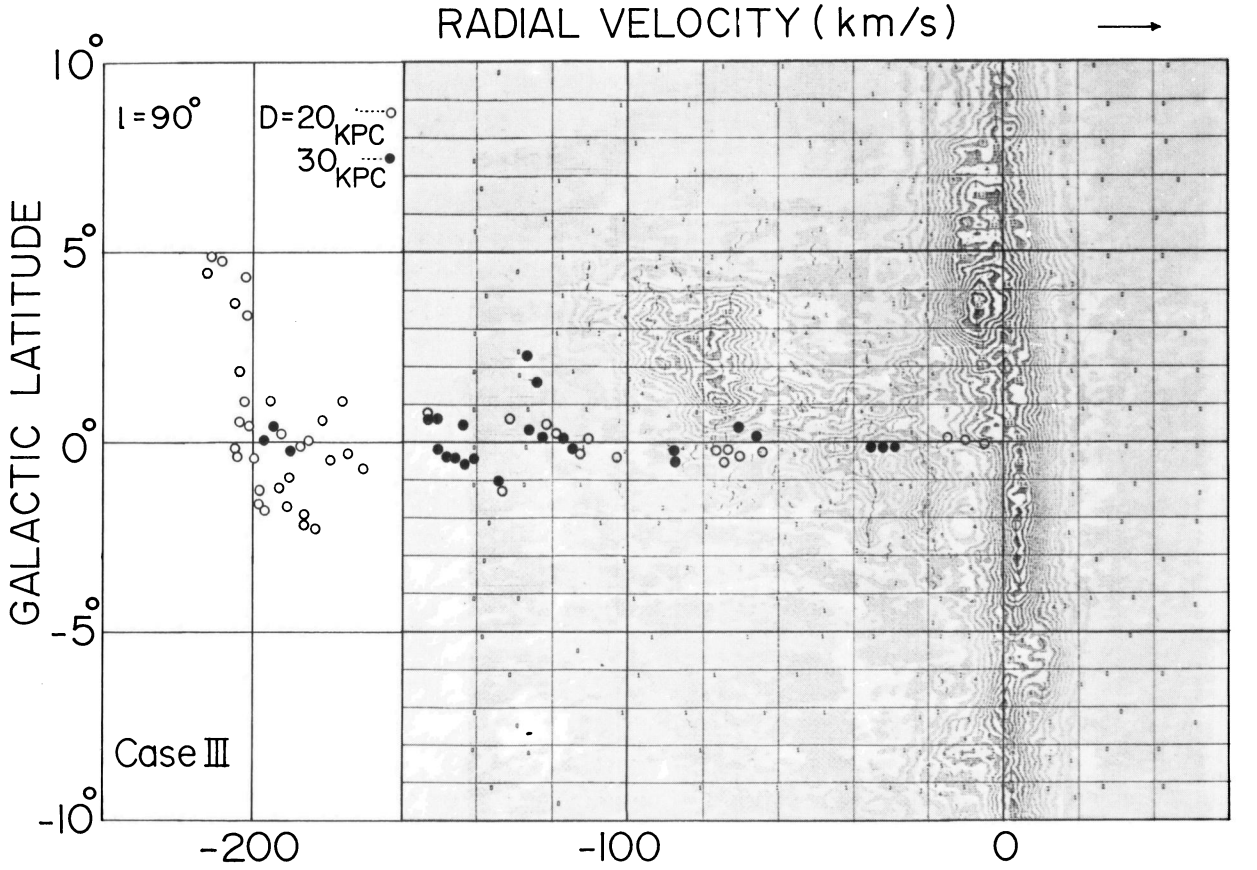


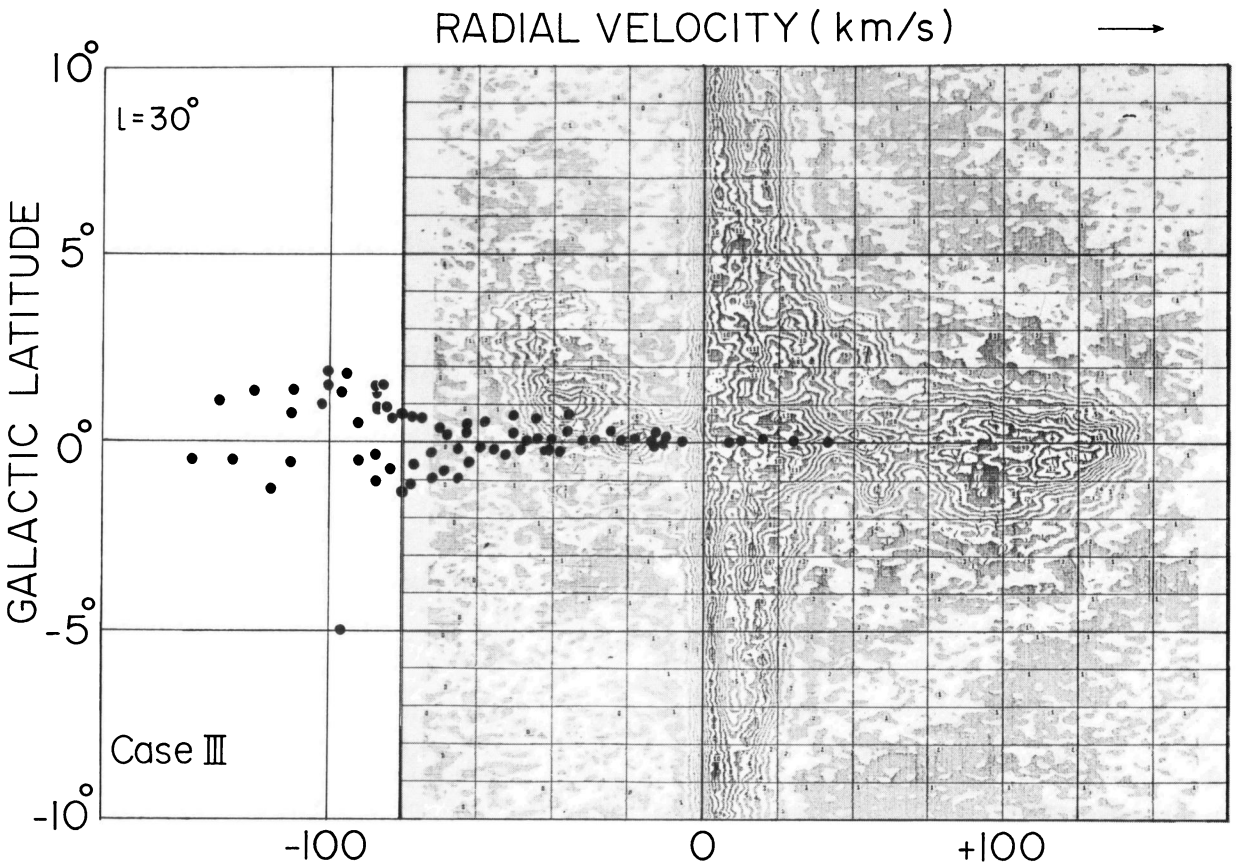


**Figs. 5a and 5b.** The computed and observed bendings of the galactic disk on the latitude-radial velocity $(b, v_r)$ diagrams at $l = 30°$ and 90°. The LMC's orbit is overhead with $D = 20$ and 30 kpc characterized by $\alpha_1$ and $\beta_1$ in Case III in Fig. 2c. The observation is after Henderson (1966)

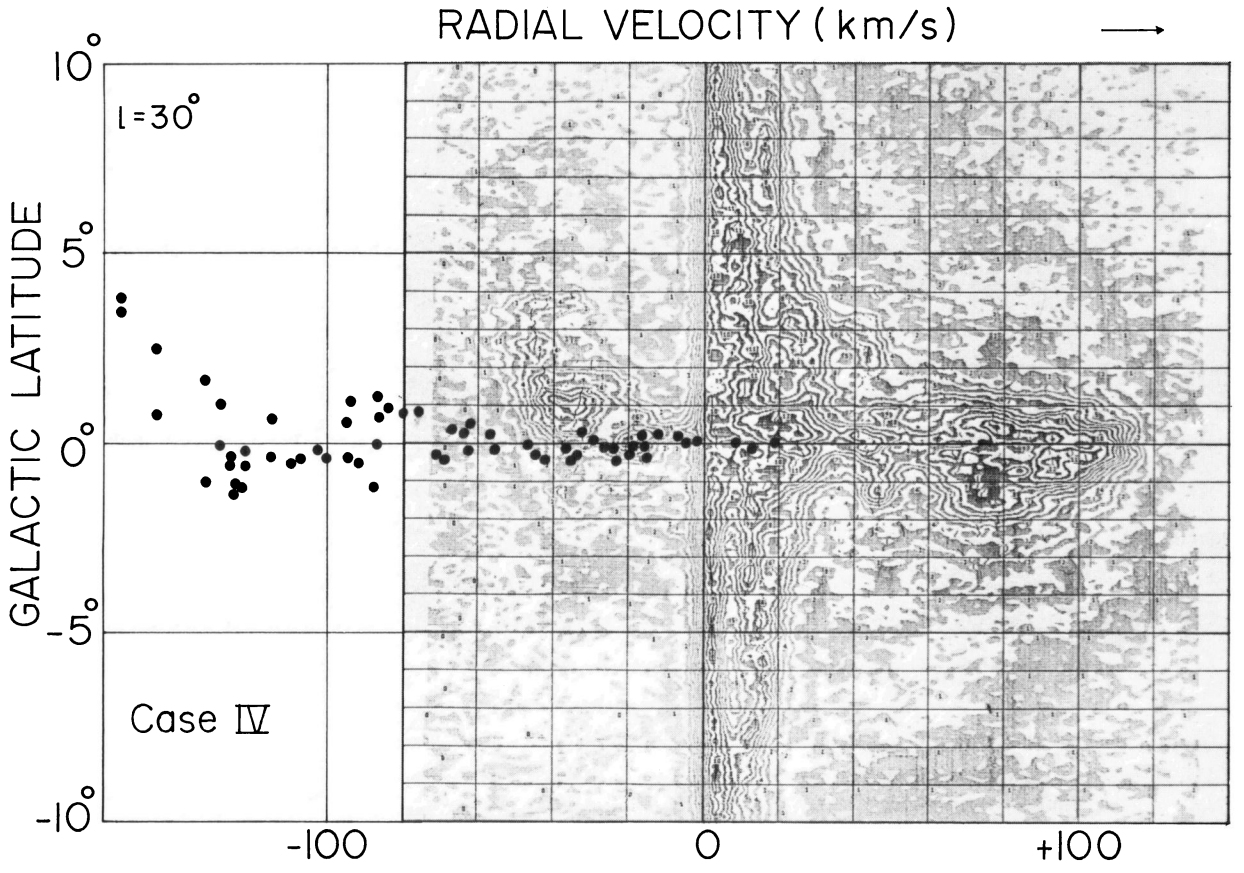


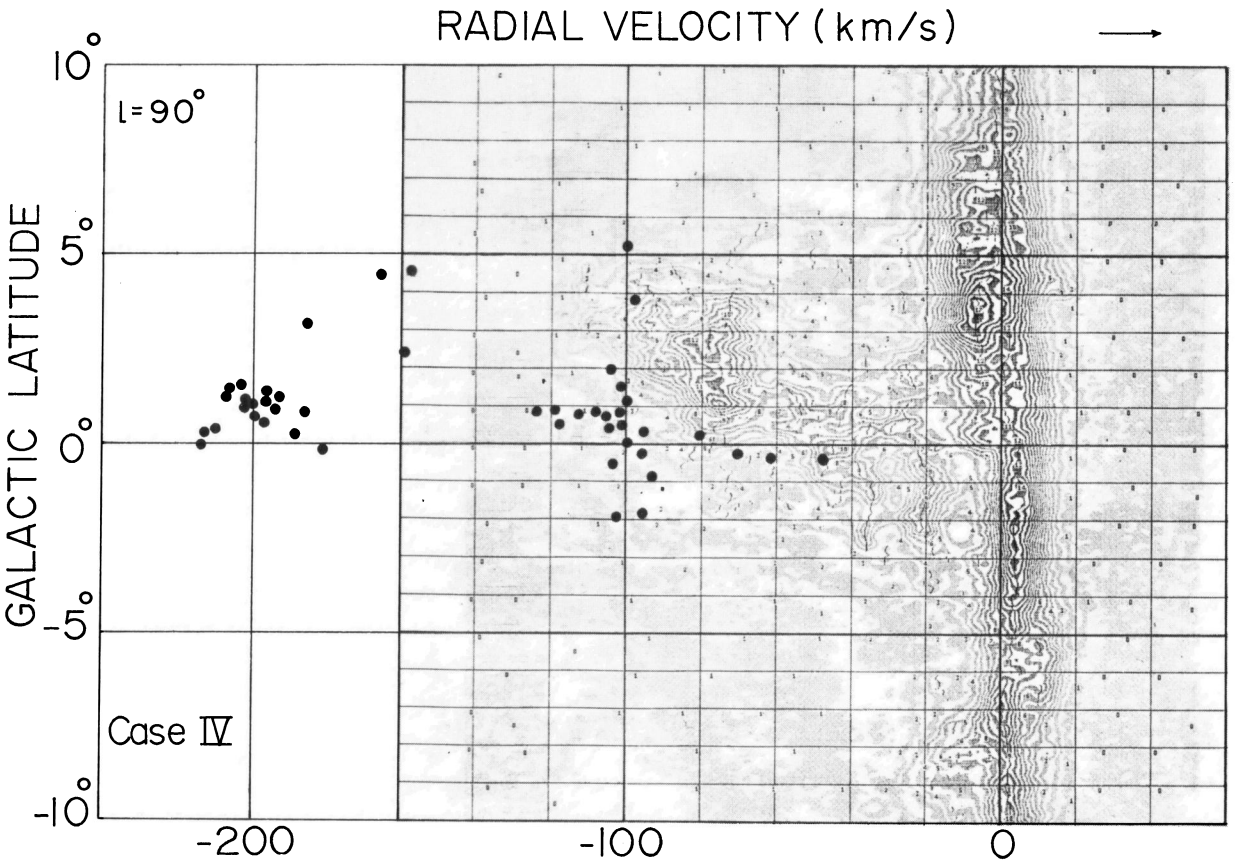


**Figs. 6a and 6b.** Same as Figs. 5a and 5b, but the LMC's orbit is overhead with $D=30$ kpc in Case IV; $m_G=1.43\,10^{11}M_\odot$, $R_0=9$ kpc and $V_0=225\,\mathrm{km\,s^{-1}}$

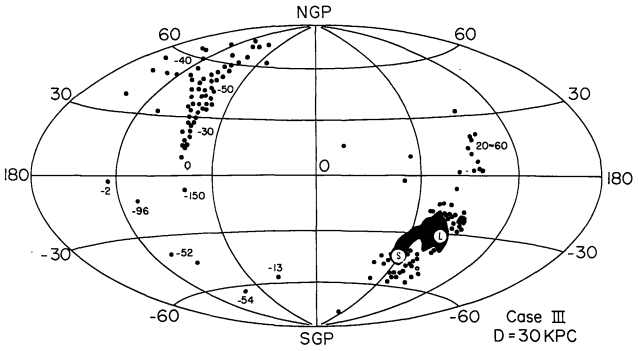


**Fig. 7a.** Present ($t=0$) distribution of the test particles on the ($l$, $b$) plane in the overhead, $D=30$ kpc orbit of the LMC in Case III ($\beta_1$ in Fig. 2c). The particles pulled out tidally from the LMC and SMC fall on a great circle on the sky, resembling the HVC, some gas-complexes at the HC region and a tail of hydrogen gas from the Clouds. Numbers show the radial velocities (km s$^{-1}$) to be observed at the Sun of the non-rotating Galaxy. The present positions of the LMC and SMC are indicated by $L$ and $S$. In the dark area, the test particles occur too close each other to be shown separately. Compare with Figure 8

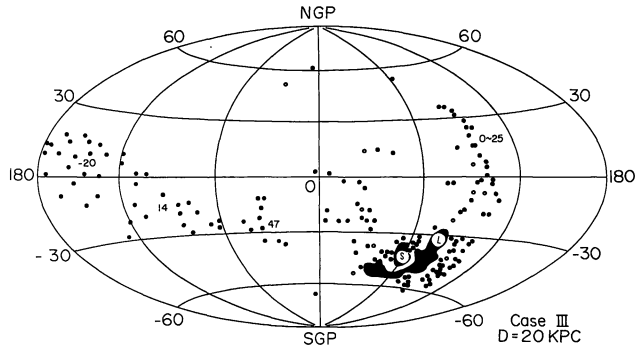


**Fig. 7b.** Similar to Figure 7a, but in the overhead, $D=20$ kpc orbit of the LMC in Case III ($\alpha_1$ in Fig. 2c). The pulled-out particles are much scattered on the sky. The HVC and the Magellanic Stream of hydrogen gas are not reproduced

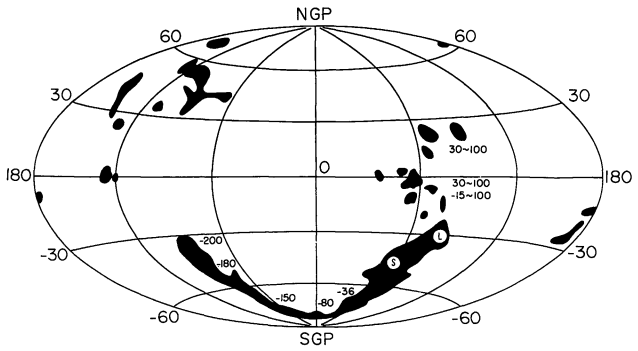


**Fig. 8.** The Magellanic Stream of hydrogen gas, high-velocity H I clouds and some H I gas complexes at $l=260°$ to 330°, $b=-20°$ to 30° (HC region) in galactic coordinates, after Mathewson et al. (1974). Numbers refer to the observed radial velocity (km s$^{-1}$) relative to the Sun of the non-rotating Galaxy. The data of Mathewson et al. have been recalculated according to our model of the Galaxy, $R_0=10$ kpc and $V_\theta=250$ km s$^{-1}$

$b=-35°$) could not be reproduced by a variety of models simulating the tidal tearing of matter from the LMC and SMC (Paper I).

In the present paper, however, we first take the earlier model of the Magellanic Stream, and try to reproduce its geometrical structure on the sky for the present choice of $m_G$, $m_L$, and $m_S$. We will then touch upon, as the second part of the present paper, the new model of the Magellanic Stream by Mathewson et al. (1974).

Continuous media of the LMC and SMC are simulated by distributing about five hundred test particles. As in Paper I, they are placed initially (when the LMC is at the apogalacticon) on eleven rings with radii 1 to 11 kpc around the center of the LMC and on eight rings with radii 1 to 8 kpc around the SMC. Again rotation was given to test particles, so that the centrifugal force balanced the gravitational forces due to the potentials (2). The planes of the LMC and SMC were taken parallel to our ($y-z$) plane (see Fig. 1), according to de Vaucouleurs' (1960) observation. We also assume that the SMC rotates in the same direction as the LMC at the initial epoch of the integration. The orbits of the LMC and SMC chosen for the following three subsections all ensure a binary state for at least the past $5\,10^9$ years.

The test particles torn off from the LMC and SMC are shown in Figure 7 projected onto the sky for two orbits of the LMC with $D=30$ and 20 kpc ($\beta_1$ and $\alpha_1$ in Fig. 2c); the SMC's orbits accompanying the LMC are characterized by the midpoints of the corresponding capture windows. Since the dynamical behavior of test particles is qualitatively the same as in Paper I, we give the result only at the present epoch for a convenient comparison with the Magellanic Stream (Fig. 8) reproduced from Mathewson et al. (1974).

When $D=30$ kpc, good reproductions are obtained of the HVC and some H I gas complexes observed at $l=270°$ to 330°, $b=-20°$ to 35° on a great circle, extrapolated from the Magellanic Stream. A few particles fall on several places corresponding to the Magellanic Stream extending from the Clouds to $l=90°$, $b=-35°$, passing near the galactic south pole.

The radial velocities (in km s$^{-1}$) averaged over nearby particles are given relative to the Sun of the non-rotating Galaxy. When $D=30$ kpc the radial velocities of the particles in the HVC region are sufficiently high to regard the particles as the high-velocity gas clouds. However, those of the particles at the Magellanic Stream are, although the sample number is small, much smaller than the observed values by about 100 km s$^{-1}$. As stated earlier, this discrepancy is exactly what Mathewson (1976) stressed in his "non-tidal" theory of the Magellanic Stream. We tried to remove this discrepancy in our tidal theory by following the test particles for other orbits of the LMC not in an overhead sense round the Galaxy ($i\neq 0$ in Table 3). The procedure was unsuccessful, for the LMC bound to the Galaxy. Indeed, the particle distributions less resemble the Magellanic Stream. No particle

**Table 4.** Summary

| | Case I | II | III | IV | Paper I | Primordial Gas Model ($D=50$ kpc) | |
|---|---|---|---|---|---|---|---|
| | | | | | | ILD** | ISD** |
| Binary orbits of the LMC and SMC | ⊙ | ⊙ | ⊙ | ⊙ | ⊙ | ⊙ | ⊙ |
| Bendings of the Galactic disk | | | | | | | |
| $D=20$, $D=30$ kpc | ● ● | ● ● | ○ ○ | ○ ○ | ● ○ | ● | ● |
| Magellanic Stream | | | | | | | |
| geometry $D=20$, $D=30$ kpc | ● ○ | — | ● ○ | ● ○ | ● ○ | ⊙ | ● |
| radial velocities | | | | | | | |
| $D=20$, $D=30$ kpc | ● ● | — | ● ● | ● ● | ● ● | ⊙ | ● |
| High-velocity HI gas*, | | | | | | | |
| geometry $D=20$, $D=30$ kpc | ● ○ | — | ● ⊙ | ● ⊙ | ● ⊙ | —† | —† |
| radial velocities | | | | | | | |
| $D=20$, $D=30$ kpc | ● ○ | — | ● ○ | ● ○ | ● ○ | —† | —† |

⊙ Compatible with observations or computationally realized (the first row)
○ Partly or qualitatively compatible with observations
● Incompatible with observations
* Computational results depend on the initial epoch at which our test particles simulations started toward the present. However, we could not find cases that black circles turn to white ones in our extensive experiments.
** ILD: Initially linear distribution; ISD: Initially spherical distribution.
† HVC are regarded as unrelated to the Magellanic Stream.

is found to fall on the portion of the Magellanic Stream passing near the galactic south pole.

As done in Paper I, even if we take into account other possible mechanisms, such as a drag force due to intergalactic gas and temporary ejection of gas from the Clouds, better agreement with the observed radial velocities at the Magellanic Stream region cannot be obtained. (See the Section VIII for the detailed effect of a drag force on the Magellanic Stream.)

When $D=20$ kpc in the same galactic model, the particles are more dispersed on the sky (Fig. 7b). Neither the HVC nor the Magellanic Stream passing by the galactic south pole could be reproduced. Thus, if the Magellanic Stream is to be explained by our tidal theory, the case of $D=20$ kpc seems to be excluded from the model of the close passage of the Magellanic Clouds.

## VII. Summary of Sections II to VI

Table 4 summarizes our extensive results in Sections II to VI by scoring the models I, II, III and IV. The results in Paper I are also given.

If we take $D=20$ to 30 kpc, particularly if $D\approx 30$ kpc in an overhead sense of Case III, many dynamical phenomena can be explained coherently in terms of the tidal interaction between the Galaxy, LMC and SMC.

We could not, however, reproduce in our tidal theory the radial velocity distribution of the Magellanic Stream trailing from the LMC and SMC. This is precisely what Mathewson et al. (1974), Mathewson (1976) and Mathewson and Schwarz (1976) stressed: they proposed that the Magellanic Stream is a diffuse primordial gas left from the condensation to the Clouds and moving on a hyperbolic orbit whose closest approach to the Galaxy is $D\approx 50$ kpc. If this is the case, aspects of our tidal theory must be largely changed.

We consider that these conflicting conclusions must be resolved not by examining only one or two aspects separately, but by synthesizing the whole situation that would be associated with the LMC-SMC system. At the same time we must search for other possible mechanisms which may produce the galactic flexure and/or remove the discrepancies at the intermediate regions of the radial velocity on the $(v_r, b)$ diagram shown in Figures 5 and 6. It should be noted also that the non-tidal theory of the Magellanic Stream has not been examined dynamically.

Bearing in mind such problems concerning the Magellanic Stream, we now turn to the primordial-gas model of the Stream, which constitutes the second part of the present paper.

## VIII. The Magellanic Stream

Following Mathewson and Schwarz (1976), we consider here that a primordial gas cloud approaches us along a hyperbolic orbit of the LMC. The orbital plane is nearly perpendicular to the line joining the Sun and the galactic center. The perigalactocentric distance that satisfies these conditions is $D\approx 50$ kpc at least for $1.2\,10^{11}\,M_\odot \lesssim m_G \lesssim 2.75\,10^{11}\,M_\odot$.

If we simply project this orbit onto the sky, it makes an arc on a great circle, spanning from $l=90°$, $b=-10°$ to $l=270°$, $b=70°$ for $m_G=2.75\,10^{11}\,M_\odot$ and from $l=88°$, $b=-32°$ to $l=270°$, $b=50°$ for $m_G=1.40\,10^{11}\,M_\odot$, in both cases passing through the present positions of the LMC and SMC and the galactic south pole. These projected orbits coincide exactly with

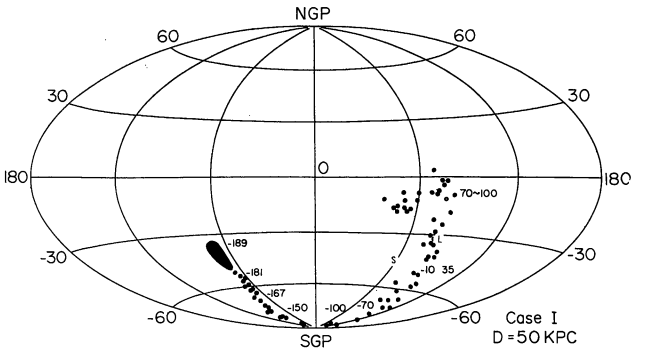


**Fig. 9a.** Present ($t=0$) distribution of test particles on the ($l$, $b$) plane in the overhead, hyperbolic orbit of the LMC in Case I ($D_1$ in Fig. 2a). About two hundred test particles were distributed initially over 200 kpc on the hyperbolic orbit of the LMC, with the LMC and SMC at the extreme end nearest the Galaxy. Local velocity corresponding to this orbit is also given to each particle. The integration of motion of each particle started when the LMC and SMC were situated 500 kpc distant from the Galaxy, and was performed forward through time to the present

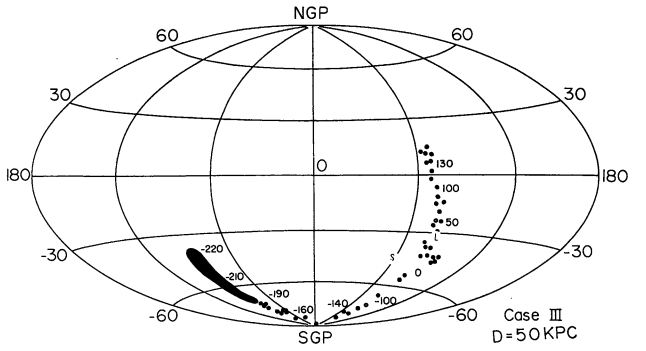


**Fig. 9b.** Similar to Figure 9a, but in Case III ($\gamma_1$ in Fig. 2c)

the Magellanic Stream in Figure 8, and the radial velocities of the nonrotating Galaxy observed from the Sun coincide with the observed values given along the Stream within a maximum deviation of $10\,\mathrm{km\,s^{-1}}$ for $m_G=2.75\,10^{11}\,M_\odot$ and $20\,\mathrm{km\,s^{-1}}$ for $m_G=1.40\,10^{11}\,M_\odot$. It is obvious that the Magellanic Clouds approached our Galaxy from the directions of the asymptotes $l=90°$, $b=-10°$ when $m_G=2.75\,10^{11}\,M_\odot$ or $l=88°$, $b=-32°$ when $m_G=1.40\,10^{11}\,M_\odot$. In this kinematical model, the HVC at $l=60°$ to 130°, $b=30°$ to 70° must be regarded as unrelated to the Stream; however, the relationship to the gas complexes at the HC region ($l=270°$ to 330°, $b=-20°$ to 35°) is not clear, because the radial velocities are too dispersed to be identified as the primodial gas moving exactly along the hyperbolic orbits.

These kinematic arguments are examined dynamically below. Special attentions are given to ascertain how the observed narrow stream has survived without being disturbed by the gravitational forces of the LMC and SMC, and why the LMC and SMC trail the narrow gas stream.

First, we placed approximately two hundred test particles in a line on the same hyperbolic orbit of the LMC, with the LMC at the end nearer the Galaxy. The LMC and each particle were given velocities sufficient to move them along the orbit. The SMC was placed in a binary orbit with the LMC. The integration commenced when the LMC was at 500 kpc distant from the Galaxy.

The particle distributions at $t=0$ for Cases I and III are shown projected onto the sky in Figures 9a and 9b. In comparison with Figure 8, we find good reproductions of the observed linear distribution of gas and its high negative radial velocity with respect to the Sun of the non-rotating Galaxy. Moreover, if such initial linear distribution of gas is realistic, the hydrogen gas complexes at the HC region ($l=270°$ to 330°, $b=-20°$ to 30°) would be regarded as primordial gas clouds: they overtook and passed the Magellanic Clouds from behind, and are now in a disordered state. The radial-velocity distribution of these test particles is rather dispersed (70 to $100\,\mathrm{km\,s^{-1}}$ for Case I), and not inconsistent with observations. Our computations also indicate that a narrow band of gas behind the LMC has been little disturbed by the gravitational force from the Clouds. A further comparison between Figures 8 and 9 suggests that Case I reproduces the velocity distribution along the Magellanic Stream better than does Case III, by 10 to $20\,\mathrm{km\,s^{-1}}$. This velocity difference may not be large enough, however, for a choice between Cases I and III to be made.

Since the average velocity of the particles is at least $150\,\mathrm{km\,s^{-1}}$ and more on a hyperbolic orbit, the presence of any intergalactic gas would create a drag force influencing the overall distribution and motion of the Magellanic Stream. As in Paper I, we assume a drag force of $-kv$, where $k$ is a constant for all particles, and $1/k$ is a decay time during which the initial velocity declines to its $1/e$, if no other force operates. When $1/k=2\,10^9$ to $6\,10^9$ years, the test particles at $t=0$ become much more condensed at both the Magellanic Clouds region and the far end of the Stream, with a large-scale gap in the distribution near the galactic south pole with an angle of 60° along the great circle as seen from the Sun.

The above distribution is not consistent with observations (Fig. 8). Therefore, if our initial linear distribution of particles represents more or less a real structure of the primordial gas, $1/k$ would exceed $6\,10^9$ years; if we tentatively assume 3 kpc as the typical diameter of gas clouds in the Stream, the density of intergalactic gas cannot exceed 1/300 of the mean density of the Stream. The observed column density of the HI gas of the Magellanic Stream is about $2\,10^{20}$ hydrogen atoms $\mathrm{cm^{-2}}$ (Mathewson et al., 1974). If we take 5 kpc as the depth of the Stream, the above reasoning gives an estimated intergalactic gas density of $4\,10^{-5}$ hydrogen atoms $\mathrm{cm^{-3}}$. This gas density is about ten times as large as the critical mass density of the expanding universe of $H=50\,\mathrm{km/s\cdot Mpc}$.

We have assumed the LMC and SMC just at the head of the Stream initially. It is presumptuous, however, to

suppose such a particular distribution of gas *a priori* and to accept the primordial gas model in the present form without providing a specific mechanism to produce the narrow band of gas. The mechanism that appears most likely at present moment is a drag force operating only on the primordial gas remaining after the condensation of the Clouds. The primordial gas would be decelerated relative to the LMC and SMC and stretched to the observed structure.

In order to examine this mechanism, we distributed initially about two hundred test particles within a huge sphere of radius of 70 kpc having the LMC and SMC at its center, and gave a random velocity of 10 km s$^{-1}$ to each particle, superimposed on the hyperbolic orbital motion. A drag force due to the intergalactic gas is assumed again as $-kv$. The computations started at $t=-2.5\,10^9$ years, when the primordial gas cloud was at 510 kpc from the Galaxy. Other orbital elements remained the same as previously. Figure 10a–c shows the numerically simulated Magellanic Stream at $t=0$ for $1/k=1.8\,10^{10}$, $6\,10^9$ and $2\,10^9$ years, respectively. A trailing structure from the LMC and SMC can indeed be recognized. However, a gap appears in the particle distribution between the Clouds and the end of the Stream, and the model Stream is too short and dispersed, particularly when $k$ is small. (The spread and depth of the particle distribution are about 25 kpc.) It is to be noted that such computed results are not observed along the Magellanic Stream whose density decreases steadily from the Clouds to the far end.

The radial velocities of the model Stream as observed at the Sun of the non-rotating Galaxy are also given along the distribution of the particles in km s$^{-1}$. Although the LMC orbit is the same as in Fig. 9b, no satisfactory agreement is obtained with the observed values given in Figure 8.

As shown in Figure 10, the particles do not follow a great circle. They are not on the orbital plane of the LMC which is approximately equal to the $(x, z)$ plane in Figure 1, but are off from it on the opposite side to the Sun ($y<0$). The distance of particles to the $(x, z)$ plane is, measured parallel to the $y$-axis, 15–45 kpc at $l\simeq 330°$, $b\simeq -45°$ to $l\simeq 60°$, $b=-60°$ of the computed Stream in Figure 10b. This displacement of particles is due to the gravitational perturbation by the LMC and mostly by the SMC. Note that the magnitude of perturbation due to the LMC and SMC is different for cases in Figures 9 and 10: the test particles were distributed initially on a line and most of them were already apart from the Clouds region in case of Figure 9.

Another important result is the deviation of particles at the arrowed regions in Figure 10a–c from the smoothed locus of the particle distribution, leading to the galactic center. Such humps in the particle distribution inevitably are associated with the assumed dynamical state that the primordial gas cloud was stretched by the drag force, $-kv$, in the gravitational potential from the

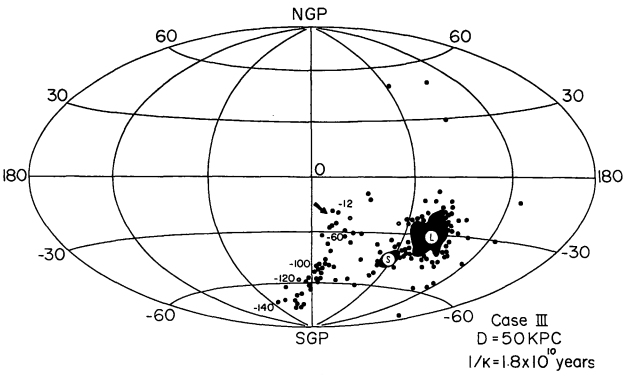


**Fig. 10a.** Present ($t=0$) distribution of the test particles on the ($l$, $b$) plane in the overhead, hyperbolic orbit of the LMC in Case III ($\gamma_1$ in Fig. 2c). A spherical distribution of test particles is assumed initially with the LMC and SMC at its center. The integration of motion of each particle started when the LMC was 510 kpc distant from the Galaxy. $1/k=1.8\,10^{10}$ years is assumed. Note a hump in the particle distribution (arrow), and a gap arising at 310° to 340°. The particles do not fall on the Magellanic Stream region adjacent to the south galactic pole

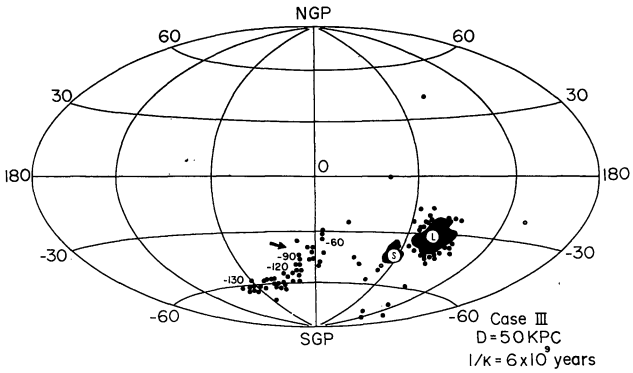


**Fig. 10b.** Similar to Figure 10a, but $1/k=6\,10^9$ years. A hump occurs in the particle distribution (arrow). The gap is more pronounced than that in Figure 10a

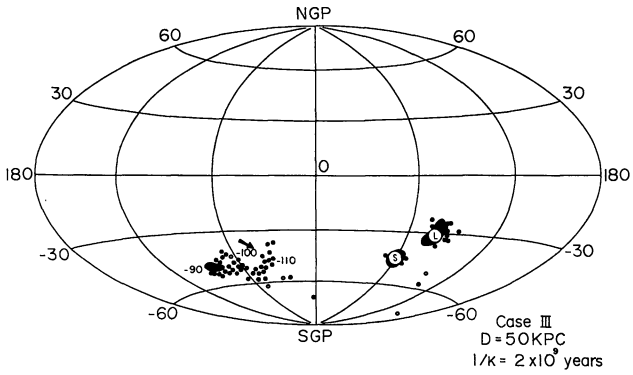


**Fig. 10c.** Similar to Figure 10a but $1/k=2\,10^9$ years. A hump is still evident in the particle distribution (arrow). Most of the particles have condensed into the LMC and SMC

Galaxy. No hump is, however, observed in the Magellanic Stream.

Moreover, if we try to reproduce a long tail comparable with observations, we must increase $k$, which, against our expectation, introduces even wider gaps between the Clouds region and the Stream end.

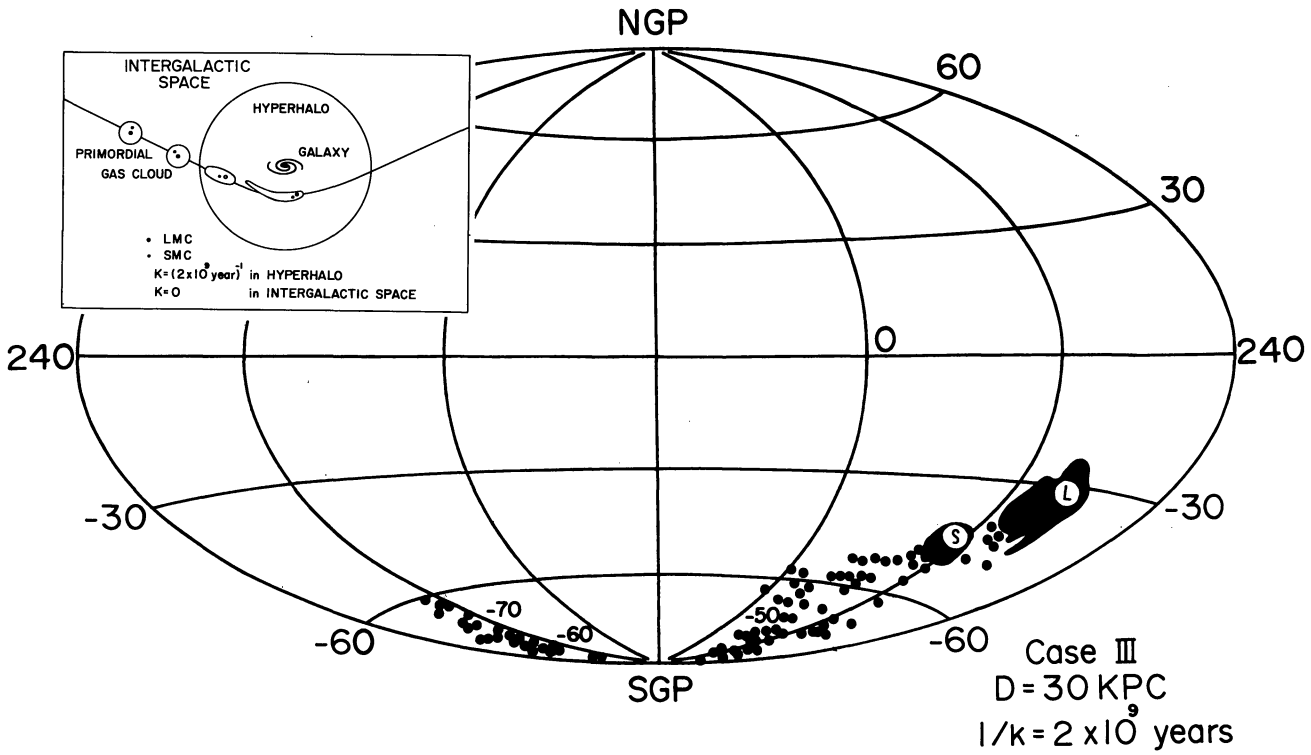


**Fig. 11.** Similar to Figure 10a, but $1/k=2\,10^9$ years in a hypothetical "hyperhalo" around the Galaxy. A spherical primordial gas cloud is stretched by the drag force due to the hyperhalo gas. The hypothetical arrangement is shown schematically in the inset

We aimed to remove these discrepancies and obtain a more realistic distribution of the particles, resembling the Magellanic Stream both geometrically and dynamically. However, the above-mentioned humps and gaps in the particle distribution cannot be removed in principle even if we take other hyperbolic orbits or different models of the Galaxy. Since we do not have a more reasonable mechanism to stretch out the spherical gas cloud, we must take another dynamical circumstance, for which we assume a spherical primordial gas cloud centered at the LMC and SMC and approaching us without being disturbed until finally entering into a hypothetical "hyperhalo" of the Galaxy. The primordial gas would be decelerated by the drag force from the hyperhalo gas and form a gaseous tail behind the LMC and SMC only near the Galaxy.

We simulate this dynamical state again by using the same cloud of test particles and a hyperbolic orbit in an overhead sense. Radius of the hyperhalo is taken as 200 kpc and the gas density is characterized by $1/k=2\,10^9$ years. The result is given in Figure 11. (We did not try the cases of $1/k=6\,10^9$ years and $2\,10^{10}$ years, because, as already known from Figures 10a and 10b these values are of too long a duration to reproduce the Magellanic stream spanning an open angle of more than 80° along the great circle on the sky.) Unfortunately we could not reproduce the Magellanic Stream. The computed stream less resembles the observed one than do those displayed in Figure 10, although the particle distribution has less gap and also passes near the galactic south pole. A small hump is still present in the particle distribution. The velocities of the particles at the south galactic pole (SGP) to the tip of the model Stream are halved as compared with the observed velocities at the corresponding positions in Figure 8: the particles proceed on different orbits from the hyperbolic orbit of the LMC. As estimated previously, the gas density of this hyperhalo is $10^{-4}$ hydrogen atoms $cm^{-3}$ for $1/k=2\,10^9$ years; about 1/100 of the observed gas density of the Stream. Note that galactic longitudes are shifted by 60° to the right in order to avoid apparent peculiar distribution of particles near the south pole in the earlier coordinates.

## IX. Discussion

We have examined a variety of models for the Magellanic Stream by applying test particle simulation to the kinematical model of Mathewson et al. (1974) and Mathewson (1976) that the Stream is primordial gaseous debris remaining after the condensation of the Clouds and now moving on a hyperbolic orbit of the LMC.

If the primordial gas could be represented by our particles distributed spherically around the LMC and SMC, the elongation of the cloud can be reproduced by a drag force due to intergalactic gas. However, a smooth locus determined from averaging the positions of the particles does not pass the galactic south pole, but deviates from it by 30° in galactic latitude. The radial

velocities along this locus are more positive than the observed ones by 40 to 50 km s$^{-1}$. Moreover, a large-scale gap and hump evident in the particle distribution are not observed along the Magellanic Stream.

Mathewson et al. (1974) emphasized the importance of the high negative radial velocities along the Stream and advocated abandoning hypotheses for a tidal origin of the Stream. Based on our extensive examinations of the model Stream, however, we stress equally that it is still quite unclear how a linear distribution of gas with no gap and hump can be derived from a primodial gas cloud of ordinary configuration.

We believe it urgent for us to find a more realistic elongation-mechanism of a primordial gas cloud, and to consider whether we should accept the non-tidal theory of the Stream at the expense of abandoning the rather good score for a tidally-flexed Galaxy of $D=30$ kpc in Case III and IV in Table 4.

*Acknowledgements.* All computations were made on a HITAC 8500 at the Institute of Plasma Physics, Nagoya University. We are indebted to Professor K. Takayama, director of the Institute, for making the computer available to us. We wish to express our hearty thanks to Dr. G. E. Williams of the BHP Melbourne Research Laboratory for his comments to and critical reading of our manuscript.

## References

Avner, E.S., King, I.R.: 1967, *Astron. J.* **72**, 650
Clutton-Brock, M.: 1972, *Astrophys. Space Sci.* **17**, 292
Davies, R.N.: 1972, *Monthly Notices Roy. Astron. Soc.* **160**, 381
de Vaucouleurs, G.: 1960, *Astrophys. J.* **131**, 265
Dieter, N.H.: 1965, *Astron. J.* **70**, 552
Einasto, J., Haud, U., Joeveer, M., Kaasik, A.: 1976, preprint
Elwert, G., Hablick, D.: 1965, *Z. Astrophys.* **61**, 273
Eneev, T.M., Kozlov, N.N., Sunyaev, R.A.: 1973, *Astron. Astrophys.* **22**, 41
Fujimoto, M., Sofue, Y.: 1976, *Astron. Astrophys.* **47**, 263
Henderson, A.P.: 1966, Latitude-Velocity Maps, College Park, University of Maryland
Hindman, J.V., Kerr, F.J., McGee, R.X.: 1963, *Australian J. Phys.* **16**, 570
Hindman, J.V.: 1967, *Australian J. Phys.* **20**, 147
Hulsbosch, A.N.M., Raimond, E.: 1966, Bull. Astron. Inst. Neth. **18**, 413
Hunter, C., Toomre, A.: 1969, *Astrophys. J.* **155**, 747
Innanen, K.A.: 1966, *Astrophys. J.* **143**, 153
Kepner, M.: 1970, *Astron. Astrophys.* **5**, 444
Kerr, F.J., Westerhout, G.: 1965, in Galactic Structure, Ed. A. Blaauw and M. Schmidt, University of Chicago press, P. 167
Lynden-Bell, D.: 1976, *Monthly Notices Roy. Astron. Soc.* **147**, in press
Mathewson, D.S., Ford, V.L.: 1970, *Astrophys. J.* **160**, L43
Mathewson, D.S., Cleary, U.N., Murray, J.C.: 1974, *Astrophys. J.* **190**, 291
Mathewson, D.S.: 1976, R. Greenwich Obs. No. 182
Mathewson, D.S., Schwarz, M.P.: 1976, *Monthly Notices Roy. Astron. Soc.* **176**, 47
Mirabel, I.F., Turner, K.C.: 1973, *Astron. Astrophys.* **22**, 437
Miyamoto, M., Nagai, R.: 1975, *Publ. Astron. Soc. Japan* **27**, 533
Nagai, R., Miyamoto, M.: 1976, *Publ. Astron. Soc. Japan* **28**, 1
Ostriker, J.P., Peebles, P.J.E.: 1973, *Astrophys. J.* **186**, 467
Pfleiderer, J., Siedentopf, H.: 1961, *Z. Astrophys.* **51**, 201
Pfleiderer, J.: 1963, *Z. Astrophys.* **58**, 12
Plummer, H.C.: 1911, *Monthly Notices Roy. Astron. Soc.* **71**, 460
Schmidt, Th.: 1970, *Astron. Astrophys.* **6**, 294
Toomre, A.: 1970, in *The Spiral Structure of our Galaxy*, IAU Symp. No. 38, Ed. B.W. Becker and G. Contopoulos, D. Reidel Publishing Co., Holland, P. 334
Toomre, A.: 1972, *Quart. J. Roy. Astron. Soc.* **13**, 241 and 266
Toomre, A., Toomre, J.: 1972, *Astrophys. J.* **178**, 623
Toomre, A.: 1973, in Mirabel and Turner (1973) given above
van Kuilenberg, J.: 1972, *Astron. Astrophys.* **16**, 276
Verschuur, G.L.: 1973, *Astron. Astrophys.* **22**, 139
Wannier, P., Wrixon, G.T.: 1972, *Astrophys. J. (Letters)* **173**, L119
Wright, A.E.: 1972, *Monthly Notices Roy. Astron. Soc.* **157**, 309
Yabushita, S.: 1971, *Monthly Notices Roy. Astron. Soc.* **153**, 97